

Article

Network Pharmacology-Based Study to Uncover Potential Pharmacological Mechanisms of Korean Thistle (*Cirsium japonicum* var. *maackii* (Maxim.) Matsum.) Flower against Cancer

Ki-Kwang Oh , Md. Adnan  and Dong-Ha Cho *

Department of Bio-Health Convergence, College of Biomedical Science, Kangwon National University, Chuncheon 24341, Korea; nivirna07@kangwon.ac.kr (K.-K.O.); mdadnan1991.pharma@gmail.com (M.A.)

* Correspondence: chodh@kangwon.ac.kr; Tel.: +82-332-506-475

Abstract: *Cirsium japonicum* var. *maackii* (Maxim.) Matsum. or Korean thistle flower is a herbal plant used to treat tumors in Korean folk remedies, but its essential bioactives and pharmacological mechanisms against cancer have remained unexplored. This study identified the main compound(s) and mechanism(s) of the *C. maackii* flower against cancer via network pharmacology. The bioactives from the *C. maackii* flower were revealed by gas chromatography-mass spectrum (GC-MS), and SwissADME evaluated their physicochemical properties. Next, target(s) associated with the obtained bioactives or cancer-related targets were retrieved by public databases, and the Venn diagram selected the overlapping targets. The networks between overlapping targets and bioactives were visualized, constructed, and analyzed by RPackage. Finally, we implemented a molecular docking test (MDT) to explore key target(s) and compound(s) on AutoDockVina and LigPlot+. GC-MS detected a total of 34 bioactives and all were accepted by Lipinski's rules and therefore classified as drug-like compounds (DLCs). A total of 597 bioactive-related targets and 4245 cancer-related targets were identified from public databases. The final 51 overlapping targets were selected between the bioactive targets network and cancer-related targets. With Kyoto Encyclopedia of Genes and Genomes (KEGG) pathway enrichment, a total of 20 signaling pathways were manifested, and a hub signaling pathway (PI3K-Akt signaling pathway), a key target (Akt1), and a key compound (Urs-12-en-24-oic acid, 3-oxo, methyl ester) were selected among the 20 signaling pathways via MDT. Overall, Urs-12-en-24-oic acid, 3-oxo, methyl ester from the *C. maackii* flower has potent anti-cancer efficacy by inactivating Akt1 on the PI3K-Akt signaling pathway.

Keywords: Akt1; cancer; *C. maackii* flower; network pharmacology; PI3K-Akt signaling pathway; Urs-12-en-24-oic acid; 3-oxo; methyl ester



Citation: Oh, K.-K.; Adnan, M.; Cho, D.-H. Network Pharmacology-Based Study to Uncover Potential Pharmacological Mechanisms of Korean Thistle (*Cirsium japonicum* var. *maackii* (Maxim.) Matsum.) Flower against Cancer. *Molecules* **2021**, *26*, 5904. <https://doi.org/10.3390/molecules26195904>

Academic Editor: Sérgio F. Sousa

Received: 4 September 2021

Accepted: 27 September 2021

Published: 29 September 2021

Publisher's Note: MDPI stays neutral with regard to jurisdictional claims in published maps and institutional affiliations.



Copyright: © 2021 by the authors. Licensee MDPI, Basel, Switzerland. This article is an open access article distributed under the terms and conditions of the Creative Commons Attribution (CC BY) license (<https://creativecommons.org/licenses/by/4.0/>).

1. Introduction

The definition of cancer is that normal cells are damaged via an aberrant endogenous process such as an abnormality during DNA replication or instability of the DNA sequence, which transforms into malignancy [1]. The DNA damage responses represent chronic inflammation via the immune signaling pathway, which results in accelerating tumorigenesis [2]. The damaged normal cells undergo cellular senescence, triggering secretion in the inflammatory cytokines leading to cellular mechanical disruption [3,4]. Because inflammation is a leading factor in causing pathological symptoms such as unknown severe pain, fatigue, and comorbidity in cancer patients, anti-inflammation strategies are thus key therapeutics [5,6]. Current anti-inflammatory agents for cancer treatment NSAIDs, including Cox-2, due to fewer adverse effects and a lower mortality rate [7]. Most commonly, anti-cancer agents aim to inhibit DNA replication and induce cancer cell death; however, cancer chemotherapeutics also attack healthy cells resulting in serious side effects

such as nausea, vomiting, hair loss, and fatigue [8–10]. On the other hand, traditional herbal plants with innovative bioactives and secondary metabolites play an essential role as effective anti-inflammatory, anti-oxidant, or anti-cancer agents [11]. For instance, plant extracts (*Urtica membranacea*, *Artemisia monosperma*, and *Origanum dayi* Post) in combination with anti-cancer drugs showed enhanced potency against specific cancer cell lines (lung, breast, colon, and prostate cancer) without exposing normal lymphocytes and fibroblasts to cytotoxicity [12]. Herbal-derived bioactives possess fewer unwanted side effects than chemotherapy, and have led to new clinical drugs such as taxol from *Taxus brevifolia* L., vincristine from *Catharanthus roseus* G. Don, and Epipodophyllotoxin from *Podophyllum peltatum* L. [12,13].

C. maackii is a perennial herbal plant, belonging to the family of *Compositae*, and is widely distributed in the mountainous areas of Korea, Japan, and China [14]. Furthermore, *Cirsium* species have been reported to have diverse pharmacological activities such as anti-oxidant, anti-inflammation, anti-cancer, and hepatoprotection effects [15–18]. Specifically, a *C. maackii* extract at a concentration of 200 µg/mL showed 36.89% inhibition against a breast cancer cell line (MDA-MB-231) [19]. Another study demonstrated that HepG2 cells treated with a MeOH extract of *C. maackii* have potent antioxidant efficacy against severe oxidant conditions [20]. Anti-inflammatory agents assist in protection against cancer development, thereby preventing cytokine storms [21]. It implies that anti-inflammatory compounds are important agonists to protect normal cells adjacent to tumor cells because they can block the overflow of cytokines. Until now, *C. maackii* flower compounds were identified by HPLC and had only been reported for anti-Alzheimer efficacy by inhibiting BACE1 [22]. Generally, the identification of polar and mid-polar compounds from extracts is based on HPLC due to its good separation capability [23,24]. From a different perspective, we utilized GC-MS analysis to discover lipophilic bioactives, which mainly act as drug-like compounds and uptake efficiently into the cells. Lipophilicity is a significant physicochemical parameter that influences membrane permeability and affinity [25]. More importantly, GC-MS, along with the molecular docking test (MDT) and ADME (Absorption, Distribution, Metabolism, and Excretion) study, is an optimal analytical method to determine drug-like compounds [26]. At present, the bioactives and mechanisms of the *C. maackii* flower against cancer remain unknown. Hence, we aimed to uncover its potential bioactives with their fundamental mechanisms through network pharmacology.

Network pharmacology (NP) as a systemic method can analyze holistic bioactive–target–disease relationships [27]. It can decipher the unknown mechanism(s) with “multiple targets”, “multiple bioactives”, instead of “one target”, “one bioactive” [28]. This approach is a very effective method to recognize the mechanism of action for lead compounds discovered from herbal plants [29]. An existing drug may be re-modelled to bind on multiple targets with the concept of NP, thus it can be a guide for drug repurposing [30]. The NP application is a powerful tool to elucidate novel targets and bioactives from natural products, and is especially effective for anti-cancer research to investigate multi-target activity in biological pathways and interaction networks [31]. Here, we implemented NP to provide key bioactive(s), uppermost target(s), and potential mechanism(s) of the *C. maackii* flower against cancer. Mainly, the flower part of herbal plants are the most underexplored part compared to other parts such as leaves, roots, and stems. During the growing season of the *C. maackii* plant, the flowering part might be utilized as a source of essential bioactives or be taken as a functional food. In this study, we suggest that *C. maackii* flowers are valuable parts with potential anti-cancer compounds.

To prove their therapeutic value, we performed a GC-MS analysis, protein network investigation, and a molecular docking test (MDT). Its brief processes are discussed below.

Firstly, bioactives from the *C. maackii* flower were identified by GC-MS analysis and screened to find drug-likeness compounds via an in silico tool. Then, targets associated with bioactives or cancer were identified through public databases, and final overlapping targets were utilized to analyze protein–protein interaction (PPI) and the highest degree of a target. Thirdly, a signaling pathway–target protein–bioactive (S–T–B) relationship against

cancer was identified by networking analysis. Lastly, we found the most potent bioactive and a hub target to alleviate cancer severity by exploring the molecular mechanism of the *C. maackii* flower based on MDT. The workflow diagram is displayed in Figure 1.

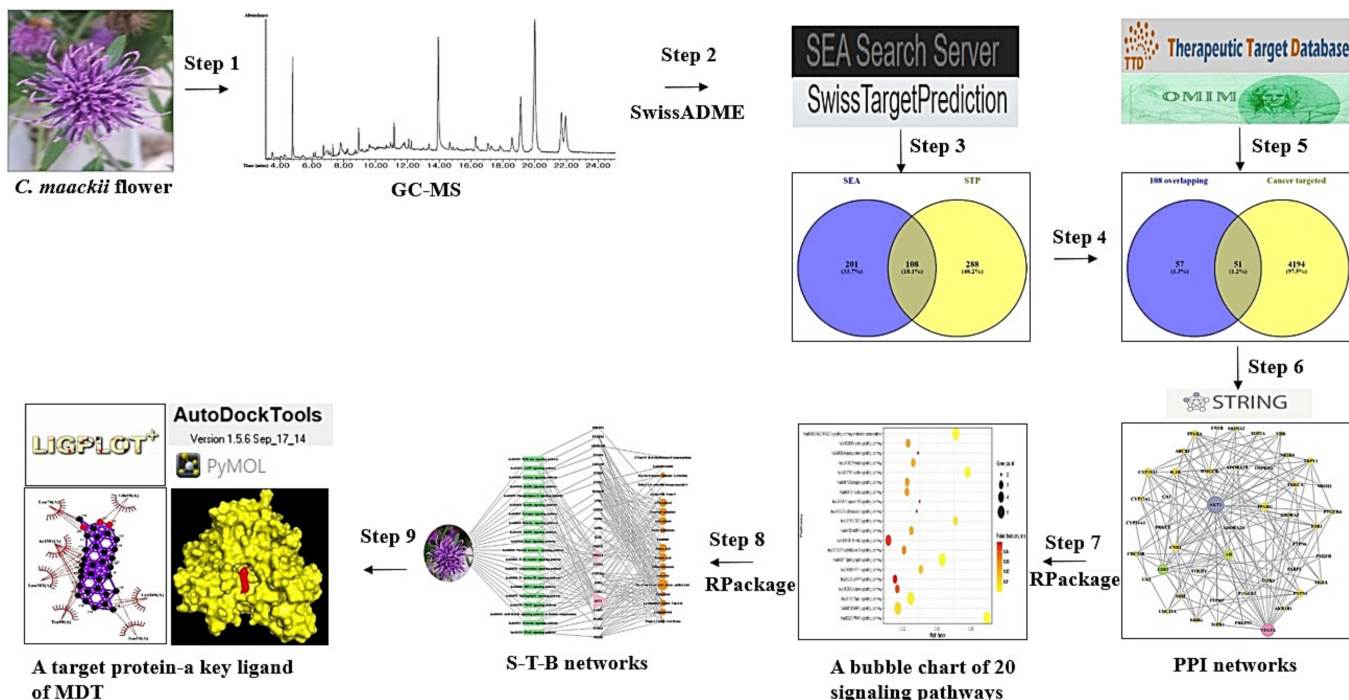


Figure 1. Workflow diagram of network pharmacology analysis of the *C. maackii* flower against cancer.

2. Results

2.1. Bioactives from *C. maackii* Flower

A total of 34 bioactives in the *C. maackii* flower were identified by GC-MS analysis (Figure 2), and the name of compounds, PubChem ID, retention time (mins), and peak area (%) are listed in Table 1. All 34 compounds were accepted by Lipinski's rules (Molecular Weight ≤ 500 g/mol; Moriguchi octanol-water partition coefficient ≤ 4.15 ; Number of Nitrogen or Oxygen ≤ 10 ; Number of NH or OH ≤ 5), and all bioactives corresponded with the standard of "Abbott Bioavailability Score (>0.1)" through SwissADME. The TPSA (Topological Polar Surface Area) value of all bioactives was also accepted (Table 2).

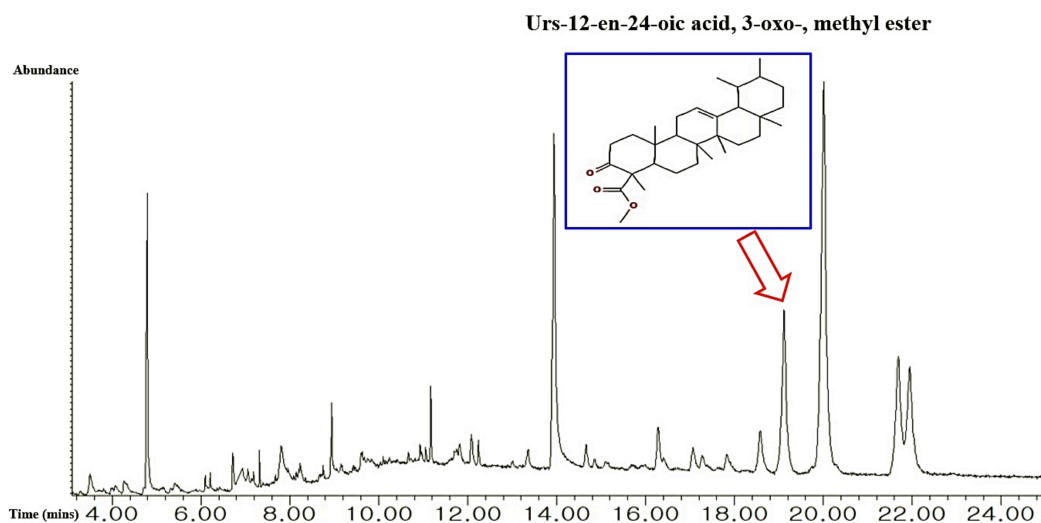


Figure 2. GC-MS peak of the *C. maackii* flower MeOH extract and an indication of the uppermost bioactive.

Table 1. A list of the 34 bioactives identified from *C. maackii* through GC-MS and profiling of bioactivities.

No.	Compounds	Pubchem ID	RT (mins)	Area (%)	Pharmacological Activities (References)
1	Glyceraldehyde	751	3.510	0.91	No reported
2	6-Methyluracil	12283	4.279	0.88	No reported
3	3-Hydroxy-2,3-dihydromaltol	119838	4.789	5.19	No reported
4	Pyranopyridine	534033	5.414	0.69	No reported
5	Formicin	69365	6.096, 6.212	0.58	No reported
6	4-Nitro-2-picoline <i>N</i> -oxide	95291	6.721	0.6	No reported
7	2-Vinyl-9- β -D-ribofuranosyl]hypoxanthine	135493011	6.933	1.35	Antibacterial and antifungal activity [32]
8	2-Chloromethyl-3,3-dichloropropene	43492	7.058	0.51	No reported
9	d-Lyxo-d-manno-nononic-1,4-lactone	535556	7.183	0.43	No reported
10	Pentyl isobutyrate	75554	7.327	0.26	Antimicrobial activity [33]
11	2-Methyl-3-nitrosooxazolidine	38357	7.673	0.23	No reported
12	<i>N</i> -Nitrosomethylethanolamine	33646	7.808	2.71	No reported
13	1,4,7,10-Tetraoxacyclododecan-2-one	533646	8.145	0.15	No reported
14	4-methylpyrimidin-2-ol	407091	8.231	0.58	No reported
15	Diethyl malonate	7761	8.750	0.46	No reported
16	Palmitic acid	985	8.943, 9.443, 9.760, 10.106	4.03	Anti-inflammation [34]
17	Methyl 3,6-anhydrohexopyranoside #	91691384	9.154	0.65	No reported
18	3-Hydroxypropionic acid	68152	9.625	1.17	Antibacterial activity [35]
19	2,2,4-Trichloro-1,3-cyclopentenedione	150757	9.846	0.65	No reported
20	Isopropyl palmitate	8907	10.673	0.54	Antibacterial activity [36]
21	Stearic acid	5281	10.933	0.72	Antibacterial activity [37]
22	Pregn-5,7-diene-3-ol-20-one	21117403	11.068	0.25	No reported
23	9-Heptadecanone	10887	11.173	0.95	Antibacterial activity [38]
24	Allyl stearate	80500	12.087	1.05	No reported
25	Squalene	638072	12.250	0.54	Anti-oxidant [39]
26	Prexanthoperol	628742	13.952	13.65	No reported
27	α -Tocopherol	14985	14.664	0.94	Anticancer [40]
28	β -Stigmasterol	6432745	16.289	1.68	Anti-inflammation [39]
29	4,4-Dimethylcholest-7-en-3-ol	5460076	17.077	1.06	No reported
30	Aristol-9-en-8-one #	6432651	17.837	1.11	No reported [39]
31	α -Amyrin	73170	18.587	2.53	Anti-obesity [41]
32	Urs-12-en-24-oic acid, 3-oxo-, methyl ester	612822	19.125	9.04	Potential Anti-inflammation [42]
33	Lupenyl acetate	323074	20.019	24.42	Antibacterial activity [43]
34	Cholesterol	5997	21.693, 21.952	15.19	Protective cell against pathogens [44]

Table 2. Physicochemical properties of bioactives for good oral bioavailability and cell membrane permeability.

No.	Compounds	Lipinski Rules				Lipinski's Violations	Bioavailability Score	TPSA (Å ²)
		MW	HBA	HBD	MLog P			
		<500	<10	≤5	≤4.15	≤1	>0.1	<140
1	Glyceraldehyde	90.08	3	2	−1.66	0	0.55	57.53
2	6-Methyluracil	126.11	2	2	−0.39	0	0.55	65.72
3	3-Hydroxy-2,3-dihydromaltol	144.13	4	2	−1.77	0	0.85	66.76
4	Pyranopyridine	133.15	2	0	0.73	0	0.55	22.12
5	Formicin	89.09	2	2	−0.85	0	0.55	49.33
6	4-Nitro-2-picoline N-oxide	154.12	3	0	−0.15	0	0.55	71.28
7	2-Vinyl-9-[.beta.-d-ribofuranosyl]hypoxanthine	294.26	7	4	−1.77	0	0.55	133.49
8	2-Chloromethyl-3,3-dichloropropene	159.44	0	0	2.81	0	0.55	0.00
9	d-Lyxo-d-manno-nononic-1,4-lactone	268.22	9	7	−3.85	1	0.55	167.91
10	Pentyl isobutyrate	158.24	2	0	2.28	0	0.55	26.30
11	2-Methyl-3-nitrosooxazolidine	116.12	3	0	−0.42	0	0.55	41.90
12	N-Nitrosomethylethanolamine	104.11	3	1	−0.89	0	0.55	52.90
13	1,4,7,10-Tetraoxacyclododecan-2-one	190.19	5	0	−0.99	0	0.55	53.99
14	4-methylpyrimidin-2-ol	110.11	2	1	−0.27	0	0.55	45.75
15	Diethyl malonate	160.17	4	0	0.6	0	0.55	52.60
16	Palmitic acid	256.42	2	1	4.19	1	0.85	37.30
17	Methyl 3,6-anhydrohexopyranoside #	176.17	5	2	−1.59	0	0.55	68.15
18	3-Hydroxypropionic acid	90.08	3	2	−0.85	0	0.85	57.53
19	2,2,4-Trichloro-1,3-cyclopentenedione	199.42	2	0	0.55	0	0.55	34.14
20	Isopropyl palmitate	298.5	2	0	4.91	1	0.55	26.30
21	Stearic acid	284.48	2	1	4.67	1	0.85	37.30
22	Pregn-5,7-diene-3-ol-20-one	314.46	2	1	3.95	0	0.55	37.30
23	9-Heptadecanone	254.45	1	0	4.55	1	0.55	17.07
24	Allyl stearate	324.54	2	0	5.25	1	0.55	26.30
25	Squalene	410.72	0	0	7.93	1	0.55	0.00
26	Prexanthoperol	314.42	3	1	2.94	0	0.55	54.37
27	Vitamin E	430.71	2	1	6.14	1	0.55	29.46
28	β-Stigmasterol	412.69	1	1	6.62	1	0.55	20.23
29	4,4-Dimethylcholest-7-en-3-ol	414.71	1	1	6.73	1	0.55	20.23
30	Aristol-9-en-8-one #	218.33	1	0	3.56	0	0.55	17.07
31	α-Amyrin	426.72	1	1	6.92	1	0.55	20.23
32	Urs-12-en-24-oic acid, 3-oxo-, methyl ester	468.71	3	0	5.92	1	0.55	43.37
33	Lupenyl acetate	144.88	2	0	7.08	1	0.55	26.30
34	Cholesterol	386.65	1	1	6.34	1	0.55	20.23

MW, Molecular Weight (g/mol); HBA, Hydrogen Bond Acceptor; HBD, Hydrogen Bond Donor; MLog P, Lipophilicity; Bioavailability Score, the ability of a drug or other substance to be absorbed and used by the body.

2.2. Overlapping Targets between SEA and STP Associated with Bioactives

A total of 309 targets from SEA and 396 targets from STP connected to 34 bioactives were identified (Supplementary Table S1). The Venn diagram showed that 108 targets overlapped between the two public databases (Supplementary Table S1) (Figure 3A).

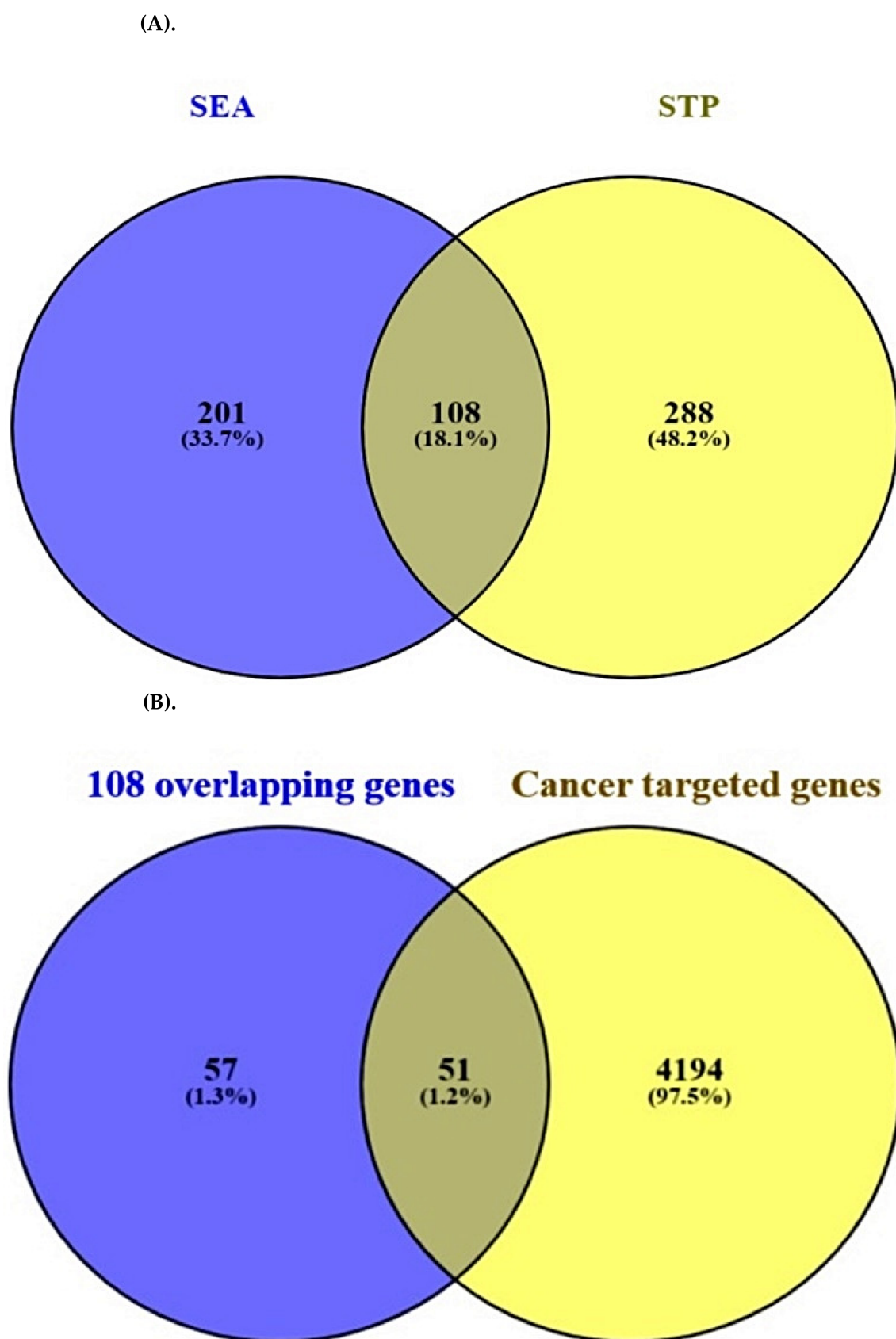


Figure 3. (A) Overlapping targets (108 targets) between SEA (309 targets) and STP (396 targets). (B) Overlapping targets (51 targets) between 108 overlapping targets from two databases (SEA and STP) and cancer associated with targets (4245 targets).

2.3. Overlapping Targets between Cancer-Associated Targets and the Final 51 Overlapping Targets

A total of 4245 targets related to cancer were selected via retrieval from TTD and OMIM databases (Supplementary Table S2). The Venn diagram results revealed 51 overlapping targets that were selected between 4245 targets associated with cancer and 108 overlapping targets (Figure 3B) (Supplementary Table S3).

2.4. Acquisition of a Hub Target from PPI Networks

From STRING analysis, 46 out of 51 overlapping targets were directly related to cancer occurrence and development, indicating 46 nodes and 145 edges (Figure 4). The five targets removed (PAM, EPHX1, PPARD, KDM5C, and BCHE) had no connectivity to the overlapping 51 targets. In PPI networks, the Akt1 target was the highest degree (29) and was considered a hub target (Table 3).

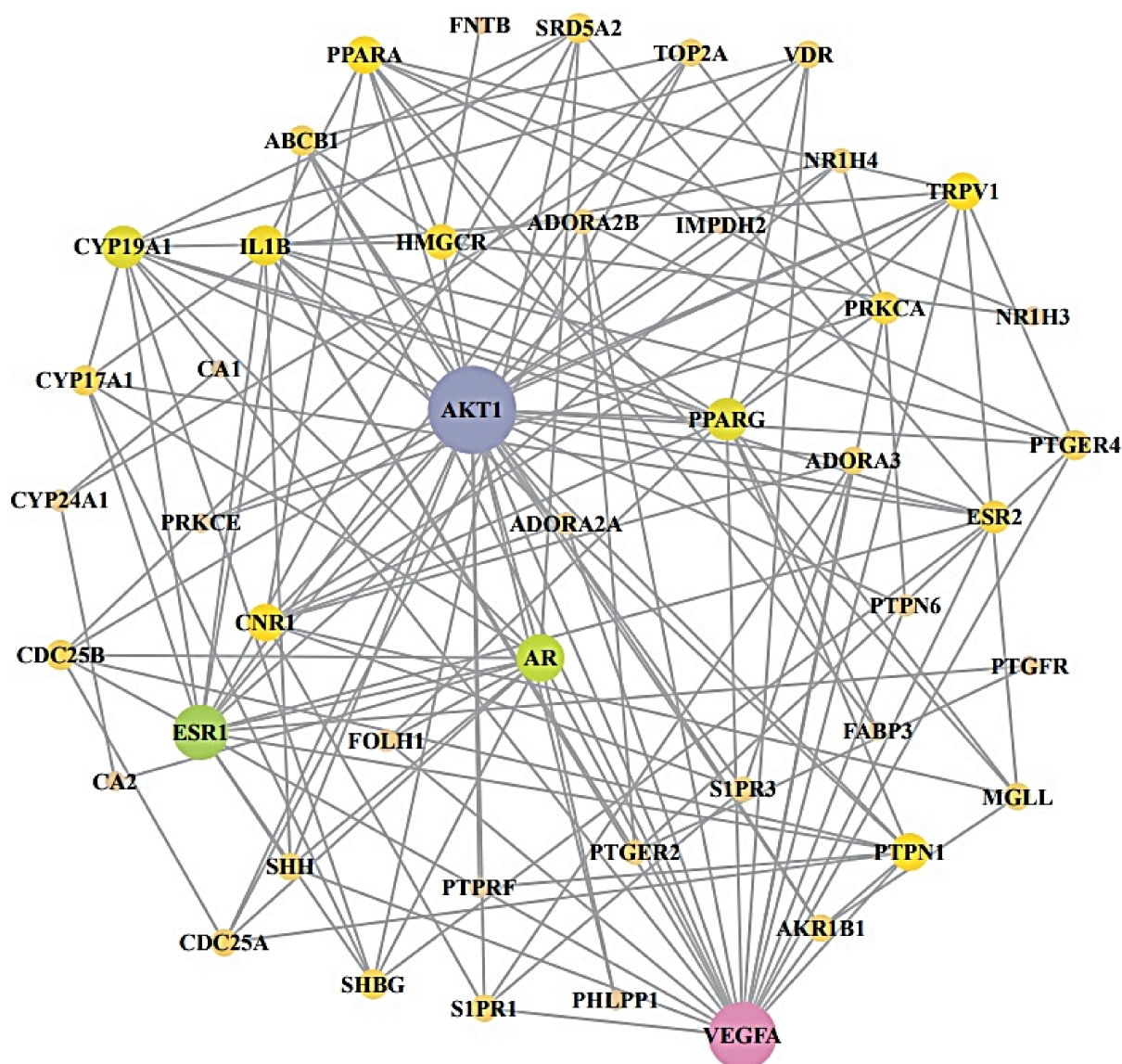


Figure 4. PPI networks (46 nodes, 145 edges). The size of circles represents the degree of values.

Table 3. The degree value of PPI networks.

No.	Target	Degree	No.	Target	Degree
1	AKT1	29	24	MGLL	5
2	VEGFA	21	25	S1PR1	5
3	ESR1	16	26	SHH	5
4	AR	13	27	VDR	5
5	CYP19A1	11	28	TOP2A	5
6	PPARG	11	29	ADORA2B	4
7	IL1B	10	30	PTGER2	4
8	CNR1	9	31	S1PR3	4
9	TRPV1	9	32	ADORA2A	3
10	PPARA	9	33	CYP24A1	3
11	PTPN1	9	34	FOLH1	3
12	HMGCR	8	35	PTPN6	3
13	ESR2	7	36	CA2	2
14	PRKCA	7	37	FABP3	2
15	ABCB1	6	38	NR1H3	2
16	CDC25B	6	39	PHLPP1	2
17	PTGER4	6	40	PTPRF	2
18	SHBG	6	41	PRKCE	2
19	CYP17A1	6	42	PTGFR	2
20	SRD5A2	6	43	CA1	1
21	ADORA3	5	44	FNTB	1
22	AKR1B1	5	45	NR1H4	1
23	CDC25A	5	46	IMPDH2	1

2.5. Identification of a Hub Signaling from Bubble Chart

The output of KEGG (Kyoto Encyclopedia of Genes and Genomes) pathway enrichment analysis revealed that 20 signaling pathways were associated with 24 targets (False Discovery Rate < 0.05). The 20 signaling pathways were directly connected to cancer, suggesting that these 20 signaling pathways might be the noteworthy pathways of the *C. maackii* flower against cancer. The descriptions of 20 signaling pathways are displayed in Table 4. Additionally, a bubble chart suggested that the PI3K-Akt signaling pathway might be a hub signaling pathway of the *C. maackii* flower against cancer (Figure 5). Among the 20 signaling pathways, the Akt1 target was associated with 18 signaling pathways, representing the highest degree of value. Most importantly, Akt1 is directly related to the PI3K-Akt signaling pathway whereas both the PPAR signaling pathway and the Calcium signaling pathway are not correlated with Akt1.

Table 4. The degree value of S-T-B networks.

No.	Target	Degree	Bioactive	Degree	No.	Target	Degree	Bioactive	Degree
1	AKT1	18	Urs-12-en-24-oic acid,3-oxo-, methyl ester	36	13	S1PR1	1	Cholesterol	14
2	PRKCA	12	Palmitic acid	27	14	S1PR3	1	Pregn-5,7-diene-3-ol-20-one	10
3	VEGFA	7	Stearic acid	26	15	PTPN6	1	Methyl 3,6-anhydro hexopyranoside #	7
4	PPARA	3	α -Tocopherol	26	16	CNR1	1	Aristol-9-en-8-one #	7
5	ESR1	3	Isopropyl palmitate	26	17	HMGCR	1	Squalene	3
6	PPARG	2	Allyl stearate	25	18	PTPN1	1	Lupenyl acetate	3
7	ESR2	2	α -Amyrin	21	19	PTPRF	1	[β -d-ribofuranosyl] hypoxanthine	1
8	PRKCE	2	9-Heptadecanone	21	20	CDC25B	1		
9	IL1B	2	β -Stigmasterol	20	21	PTGFR	1		

Table 4. Cont.

No.	Target	Degree	Bioactive	Degree	No.	Target	Degree	Bioactive	Degree
10	NR1H3	1	4,4-Dimethyl-cholest-7-en-3-ol	20	22	ADORA2B	1		
11	FABP3	1	Pentyl isobutyrate	17	23	PTGER2	1		
12	CYP17A1	1	d-Lyxo-d-manno-nononic-1,4-lactone	15	24	PHLPP1	1		

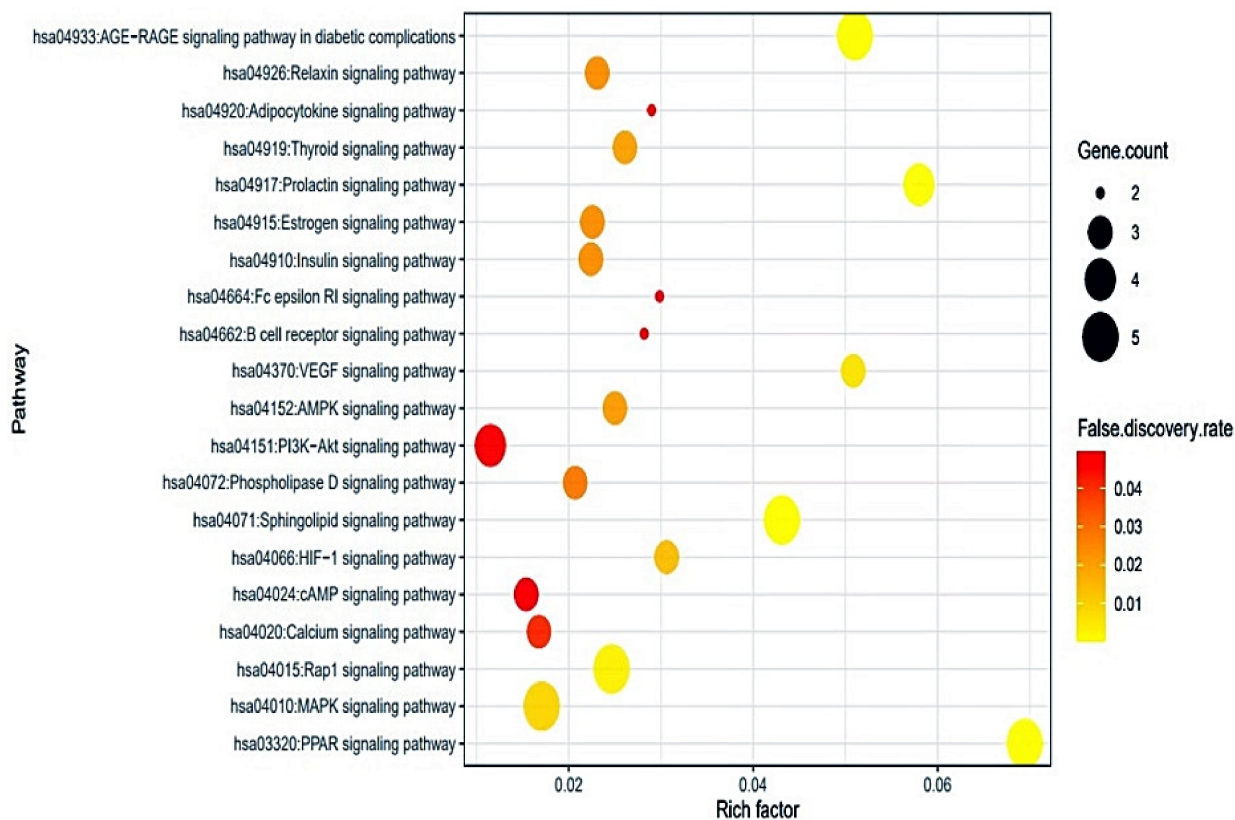


Figure 5. Bubble chart of 20 signaling pathways connected to cancer.

2.6. S–T–B Network Analysis of *C. maackii* Flower against Cancer

The S–T–B network of the *C. maackii* flower is exhibited in Figure 6. There were 20 pathways, 24 targets, and 19 bioactives (63 nodes and 204 edges). The nodes represented a total of three elements: Signaling pathways–Target protein–Bioactive (S–T–B). The edges represented relationships of a total number of three elements. The S–T–B relationship suggested that the network might interact with therapeutic efficacy against cancer. Regarding the 20 signaling pathways, the highest degree among targets was “Akt1” with 18 degrees, and the highest degree among bioactives was “Urs-12-en-24-oic acid, 3-oxo-, methyl ester” with 36 degrees (Table 5).

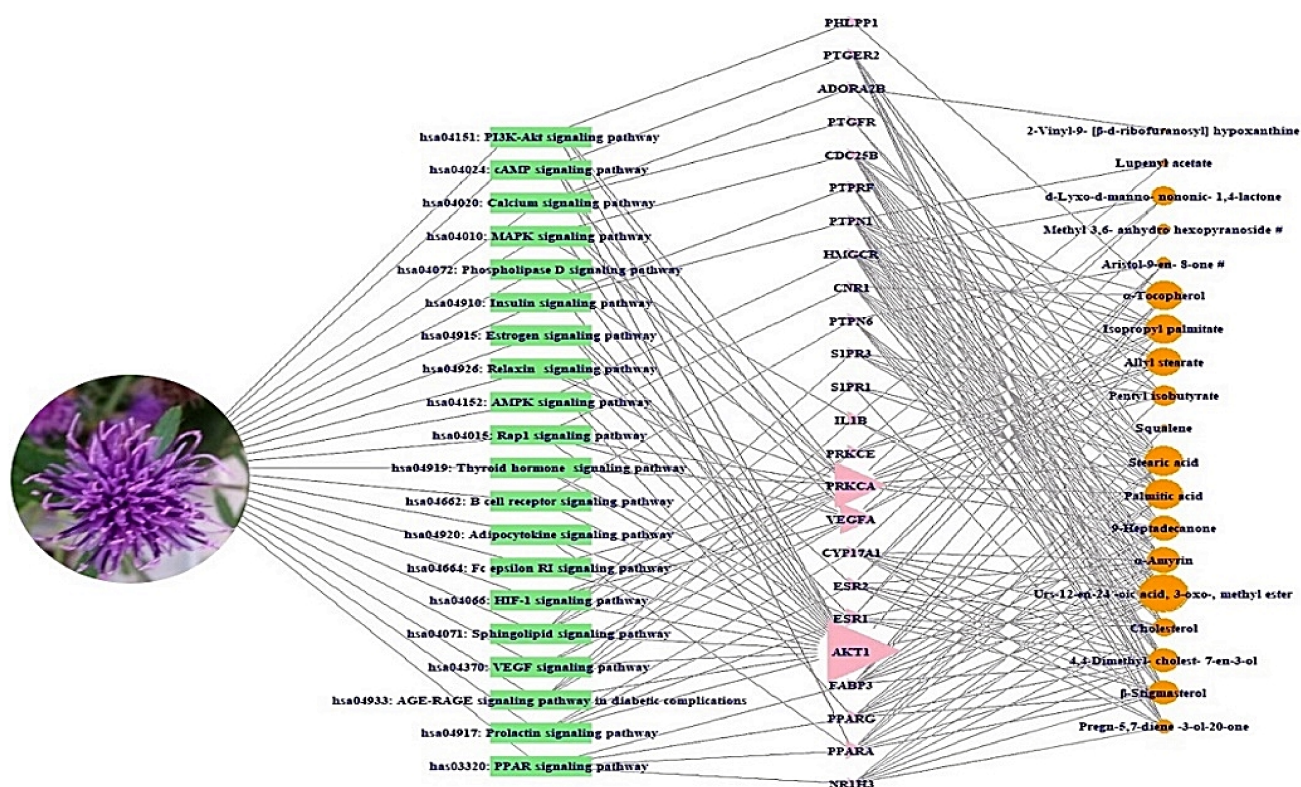


Figure 6. S–T–B networks (63 nodes, 204 edges). Green rectangle: Signaling pathway; pink triangle: Target protein; orange circle: Bioactive.

Table 5. Targets in 20 signaling pathways' enrichment related to cancer.

KEGG ID & Description	Targets	False Discovery Rate
hsa03320: PPAR signaling pathway	PPARA, PPARD, PPARG, NR1H3, FABP3	0.0000695
hsa04917: Prolactin signaling pathway	AKT1, ESR1, ESR2, CYP17A1	0.00063
hsa04933: AGE-RAGE signaling pathway in diabetic complications	AKT1, VEGFA, PRKCA, PRKCE, IL1B	0.00018
hsa04370: VEGF signaling pathway	AKT1, VEGFA, PRKCA	0.0068
hsa04071: Sphingolipid signaling pathway	AKT1, VEGFA, PRKCE, S1PR1, S1PR3	0.00027
hsa04066: HIF-1 signaling pathway	AKT1, VEGFA, PRKCA	0.016
hsa04664: Fc epsilon RI signaling pathway	AKT1, PRKCA	0.0492
hsa04920: Adipocytokine signaling pathway	AKT1, PPARA	0.0492
hsa04662: B cell receptor signaling pathway	AKT1, PTPN6	0.0492
hsa04919: Thyroid signaling pathway	AKT1, ESR1, PRKCA	0.0236
hsa04015: Rap1 signaling pathway	AKT1, VEGFA, PRKCA, VEGFA, ADORA2B	0.003
hsa04152: AMPK signaling pathway	AKT1, PPARG, HMGCR	0.025
hsa04926: Relaxin signaling pathway	AKT1, VEGFA, PRKCA	0.0278
hsa04915: Estrogen signaling pathway	AKT1, ESR1, ESR2	0.0279
hsa04910: Insulin signaling pathway	AKT1, PTPN1, PTPRF	0.0279
hsa04072: Phospholipase D signaling pathway	AKT1, PRKCA	0.0324
hsa04010: MAPK signaling pathway	AKT1, VEGFA, PRKCA, IL1B	0.0103
hsa04020: Calcium signaling pathway	PRKCA, ADORA2B	0.0457
hsa04024: cAMP signaling pathway	AKT1, PPARA, PTGER2	0.0492
hsa04151: PI3K-Akt signaling pathway	AKT1, VEGFA, PRKCA, PHLPP1	0.0487

2.7. MDT of 3 Targets and 10 Bioactives Connected to PI3K-Akt Signaling Pathway

The Akt1 protein was related to two bioactives (Urs-12-en-24-oic acid, 3-oxo-, methyl ester and α -Tocopherol), the VEGFA target to three bioactives (Allyl stearate, Isopropyl palmitate, and Methyl 3,6-anhydro hexopyranoside #), and the PRKCA target with seven

bioactives (Allyl stearate, Isopropyl palmitate, Pentyl isobutyrate, 9-Heptadecanone, Palmitic acid, Stearic acid, and d-Lyxo-d-manno-nononic-1,4-lactone). MDT was performed to verify the affinity of target protein(s) and bioactive(s), which displayed the docking figure of a hub target—the uppermost bioactive (Figure 7). The Akt1 protein (PDB ID: 5KCV) connected to two compounds on the PI3K-Akt signaling pathway was subjected to MDT. It was observed that Urs-12-en-24-oic acid, 3-oxo-, methyl ester (−12.8 kcal/mol) docked on the Akt1 protein (PDB ID: 5KCV) manifested the highest binding energy, followed by α -Tocopherol (−5.8 kcal/mol). The docking detail results of two bioactives are shown in Table 6. The MDT score of three bioactives on the VEGFA protein (PDB ID: 3V2A) was analyzed in the “Homo Sapiens” mode. It was revealed that Methyl 3,6-anhydro hexopyranoside # (−5.2 kcal/mol) docked on the VEGFA protein (PDB ID: 3V2A) exhibited the highest binding energy followed by Allyl stearate (−5.1 kcal/mol) and Isopropyl palmitate (−5.1 kcal/mol). The docking detail results of three bioactives are shown in Table 7. The MDT score of seven bioactives on the PRKCA protein (PDB ID: 3IW4) was analyzed in the “Homo Sapiens” mode. It was exposed that d-Lyxo-d-manno-nononic-1,4-lactone (−6.9 kcal/mol) docked on the PRKCA protein (PDB ID: 3IW4) demonstrated the highest binding energy, followed by Isopropyl palmitate (−6.3 kcal/mol), Stearic acid (−6.2 kcal/mol), Allyl stearate (−6.2 kcal/mol), 9-Heptadecanone (−5.4 kcal/mol), Pentyl isobutyrate (−5.0 kcal/mol), and Palmitic acid (−4.8 kcal/mol). The docking detail results of seven bioactives are shown in Table 8. Collectively, both VEGFA (PDB ID: 3V2A) and PRKCA proteins (PDB ID: 3IW4) showed that the affinity of each bioactive did not give a valid binding score (> -7.0 kcal/mol) [45].

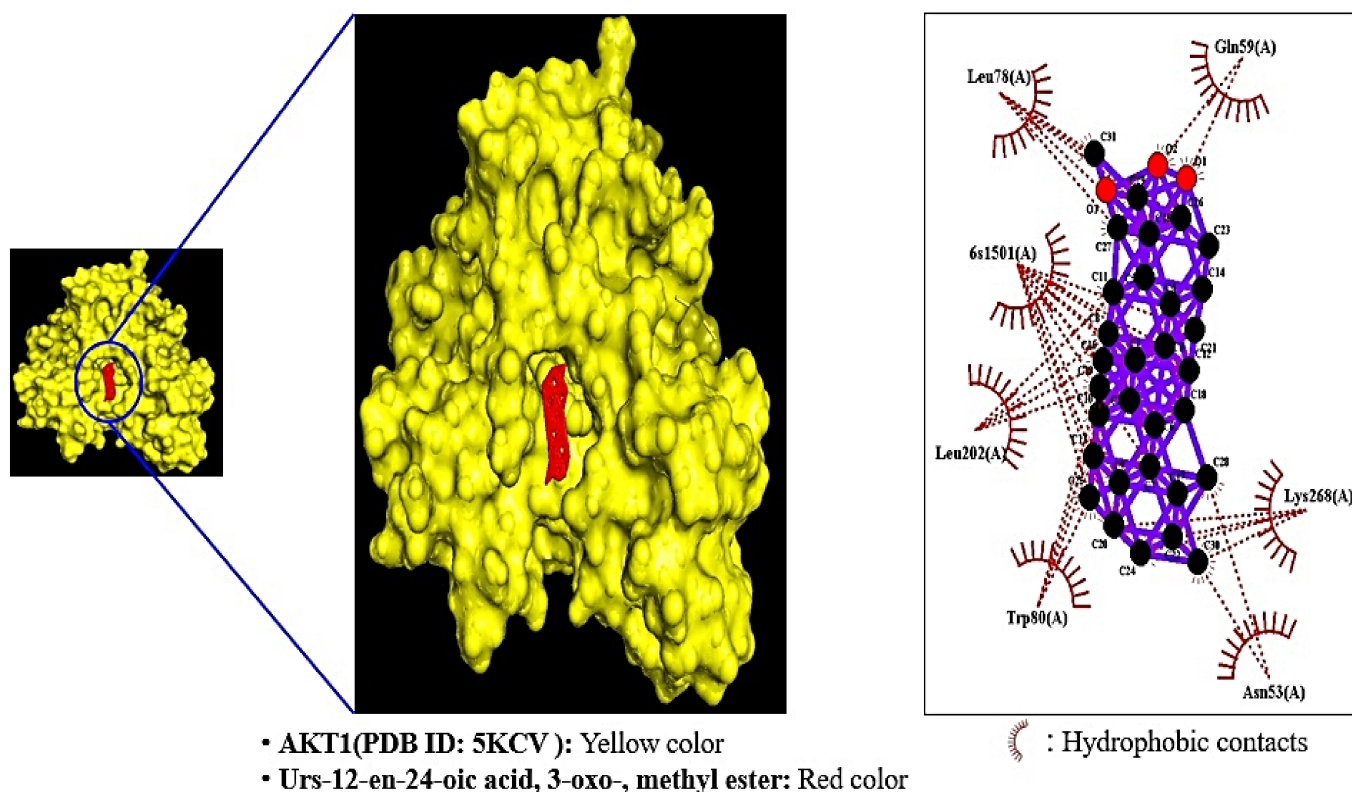


Figure 7. MDT of Urs-12-en-24-oic acid, methyl ester on Akt1 (PDB ID: 5KCV).

Table 6. Binding energy of potential bioactives on Akt1 (PDB ID: 5KCV).

Protein	Ligand	PubChem ID	Binding Energy (kcal/mol)	Amino Acid Residue	Hydrogen Bond Interactions		Hydrophobic Interactions
					R Group(s) Involved in Hydrogen Bonding	Distance (Å)	Amino Acid Residue
5KCV	Urs-12-en-24-oic acid, 3-oxo-, methyl ester	612822	−12.8	N/A	N/A	N/A	Gln59, Lys268, Asn53
	α-Tocopherol	14985	−5.8	Leu78	R-OH	2.71	Trp80, Leu202, Leu78 Ala58, Val270, Lys268 Val201, Leu202, Gln203 Trp80, Asn53

Table 7. Binding energy of potential bioactives on VEGFA (PDB ID: 3V2A).

Protein	Ligand	PubChem ID	Binding Energy (kcal/mol)	Amino Acid Residue	Hydrogen Bond Interactions		Hydrophobic Interactions
					R Group(s) Involved in Hydrogen Bonding	Distance (Å)	Amino Acid Residue
3V2A	Allyl stearate	80500	−5.1	Phe47	RCOOR'	3.18	Ile46, Lys48, Lys286 Asp276, Arg275, Pro40 Phe36
	Isopropyl palmitate	8907	−5.1	N/A	N/A	N/A	Asp276, Asp34, Ile46 Phe47, Lys48, Lys286 Phe36, Pro40
	Methyl 3,6-anhydro hexopyranoside #	91691384	−5.2	Ser310, Pro85	R-O-R', R-OH	2.98, 3.23, 2.82	Lys84, Gln87, Gly312 Asp257, Gly255, Ile256 Glu44

Table 8. Binding energy of potential bioactives on PRKCA (PDB ID: 3IW4).

Protein	Ligand	PubChem ID	Binding Energy (kcal/mol)	Amino Acid Residue	Hydrogen Bond Interactions		Hydrophobic Interactions
					R Group(s) Involved in Hydrogen Bonding	Distance (Å)	Amino Acid Residue
3IW4	Allyl stearate	80500	−6.2	Lys 396	RCOOR'	3.21	Asp395, Leu393, Pro397 Arg608, Pro398, Val664 Pro666, Ser473, Glu474 His665, Lys478, Ile667 Gln402, Asn660
	Isopropyl palmitate	8907	−6.3	Asn660	RCOOR'	2.92	Asp395, Leu393, Pro397 Lys396, Gln402, Pro398 Arg608, Ile667, Pro666 Val664, His665, Lys478
	Pentyl isobutyrate	75554	−5.0	N/A	N/A	N/A	Pro502, Gln650, Ile645 Gly540, Asp542, Asp503 Asp539, Gln642, Leu546 Glu543
	9-Heptadecanone	10887	−5.4	Lys478	RCOR'	2.80	Asn607, Gln548, Pro398 Arg608, Ile667, Tyr419 Asn421, Ser473, Pro666 Glu418, Asp472, His665 Val664, Gln402, Glu552
	Palmitic acid	985	−4.8	Asn660, Lys396	RCOR', R-OH	2.93, 2.95	Val664, Pro398, Glu552 Gln662, Asp395, Leu393 Leu394, Gln402, Pro397
	Stearic acid	5281	−6.2	Lys396, Leu393	R-OH	3.04, 2.95	Leu394, Gln402, Pro398 Lys478, His665, Ile667 Pro666, Val664, Arg608 Pro397, Asn660
	d-Lyxo-d-manno-nononic-1,4-lactone	535556	−6.9	Leu393, Lys396, Pro397 Gln402	RCOOR', R-OH	3.30, 2.73, 3.31 3.23, 3.19, 2.66 3.08, 3.03, 3.15 3.26, 2.88	Leu394, Asp395, Gln662 Asn660, Pro398

2.8. Comparative Analysis of MDT against Positive Controls on a Hub Target

A key bioactive (Urs-12-en-24-oic acid, 3-oxo-, methyl ester) associated with the PI3K-Akt signaling pathway revealed the greatest binding score (−12.8 kcal/mol) on Akt1 (PDB ID: 5KCV). The 13 positive controls on Akt1 (PDB ID: 5KCV) are as follows. The MDT score of BAY1125976 (PubChem ID: 70817911) was the highest score with −9.1 kcal/mol, followed by Miransertib (PubChem ID: 53262401; −9.0 kcal/mol), Akti-1/2 (PubChem ID: 135398501; −8.9 kcal/mol), Oridonin (PubChem ID: 5321010; −8.3 kcal/mol), MK-2206 dihydrochloride (PubChem ID: 46930998; −7.8 kcal/mol), AT7867 (PubChem ID: 11175137; −7.6 kcal/mol), A-674563 (PubChem ID: 11314340; −7.6 kcal/mol), Gsk-690693 (PubChem ID: 16725726; −7.4 kcal/mol), Ipatasertib (PubChem ID: 24788740; −7.3 kcal/mol), Capiwasertib (PubChem ID: 25227436; −7.1 kcal/mol), AT13148 (PubChem ID: 24905401; −6.9 kcal/mol), Afuresertib (PubChem ID: 46843057; −6.9 kcal/mol), and Uprosertib (PubChem ID: 51042438; −6.8 kcal/mol), respectively. In particular, the MDT score of Urs-12-en-24-oic acid, 3-oxo-, methyl ester on Akt1 (PDB ID: 5KCV) had a higher affinity (−12.8 kcal/mol) compared to the 13 positive controls. Detailed information is listed in Table 9.

Table 9. Binding energy of the positive controls on Akt1 (PDB ID: 5KCV).

Protein	Ligand	PubChem ID	Binding Energy (kcal/mol)	Amino Acid Residue	Hydrogen Bond Interactions	Distance (Å)	Hydrophobic Interactions
					R Group(s) Involved in Hydrogen Bonding		Amino Acid Residue
5KCV	MK-2206 dihydrochloride	46930998	−7.8	N/A	N/A	N/A	Leu78, Leu202, Gln203 Lys268, Trp80, Ala58, Gln59
	Gsk-690693	16725726	−7.4	Tyr18, Asp274	RNR',RNHH	3.18, 3.06	Glu85, Phe161, Val83 Cys296, Gly294, Phe293 Lys276, Leu316, Pro313 Arg273, Leu295, Ile84
	Ipatasertib	24788740	−7.3	N/A	N/A	N/A	Lys268, Asn53, Gln79 Ala58, Phe225, Leu223 Leu202, Leu78, Trp80
	Capiwasertib	25227436	−7.1	Val83	ROH	2.95	Ile84, Arg273, Asn279 Asp274, Thr291, Glu278 Phe293, Gly294, Cys296 Glu85, Glu17
	AT7867	11175137	−7.6	Ser56	RNH	3.04	Lys268, Trp80, Asn53 Leu78, Cys60, Gln79 Ala58, Cys77, Val201 Leu202, Gln203

Table 9. Cont.

Protein	Ligand	PubChem ID	Binding Energy (kcal/mol)	Amino Acid Residue	Hydrogen Bond Interactions	Distance (Å)	Hydrophobic Interactions
					R Group(s) Involved in Hydrogen Bonding		Amino Acid Residue
	A-674563	11314340	−7.6	Gln79, Gln203	RNHH, RNH	3.16, 3.20	Ser56, Trp80, Leu202 Lys268, Asn53, Ala58 Leu78
	Miransertib	53262401	−9.0	Gln203, Leu78	RNHH	3.19, 3.22	Lys268, Trp80, Leu202 Phe225, Ser216, Val201 Gln59, Gln79, Ala58
	BAY1125976	70817911	−9.1	Asp274	RNHH	3.29	Gly294, Thr291, Glu278 Asn279, Tyr229, Leu156 Glu234, Phe293, Lys158 Cys296
	Akti-1/2	135398501	−8.9	Cys296, Arg15	RCOR', RNR'	3.03, 3.15, 3.19	Glu278, Gly294, Leu295 Val83, Gln85, Glu17 Tyr18, Ile84, Phe293 Asn279
	Uprosertib	51042438	−6.8	Cys296, Leu295, Glu278	RCOR', RCOR', RNHH	2.93, 2.86, 2.93	Tyr18, Arg273, Asp274 Lys276, Thr291, Phe293 Asn279, Gly294, Ile84 Thr82
	Afuresertib	46843057	−6.9	Gly394, Gly395	RNHH	3.10, 2.95	Ala50, Arg328, Lys389 Pro388, Ala329, Asp325 Gly327, Tyr326, Phe55 Ile36, Leu52, Pro51
	AT13148	24905401	−6.9	Glu341, Tyr315, His354	ROR', ROR', RNR'	3.01, 2.70, 3.14	Phe236, Glu278, Leu347 Pro313, Tyr350, Glu314
	Oridonin	5321010	−8.3	Asp325, Ala50, Arg328	RCOR', ROH, ROH, ROH	2.67, 2.71, 2.80, 3.24	Phe55, Ile36, Leu52 Gly394, Ala329, Gly327 Tyr326

2.9. Toxicological Properties of a Selected Key Bioactive

Additionally, the toxicological properties of Urs-12-en-24-oic acid, 3-oxo-, methyl ester were predicted by the admetSAR online tool. Our result suggested that the bioactive did not disclose Ames toxicity, carcinogenic properties, acute oral toxicity, or rat acute toxicity properties (Table 10).

Table 10. Toxicological properties of the uppermost bioactive on AKT1 (PDB ID: 5KCV) in MDT.

Parameters	Compound Name Urs-12-en-24-oic acid, 3-oxo-, Methyl Ester
Ames toxicity	NAT
Carcinogens	NC
Acute oral toxicity	III
Rat acute toxicity	2.1675

AT: Ames toxic; NAT: Non-Ames toxic; NC: Non-carcinogenic; Category-II means (50 mg/kg > LD50 < 500 mg/kg); Category-III means (500 mg/kg > LD50 < 5000 mg/kg).

3. Discussion

The S–T–B network suggested that the therapeutic efficacy of the *C. maackii* flower against cancer was directly associated with 20 signaling pathways, 24 targets, and 19 bioactives. Through the network, we identified the most significant protein (Akt1) associated with the occurrence and development of cancer and a bioactive (Urs-12-en-24-oic acid, 3-oxo-, methyl ester) from the *C. maackii* flower. From a bubble chart, we identified a hub signaling pathway (PI3K-Akt signaling pathway) connected to the Akt1 target, indicating the lowest rich factor among 20 signaling pathways. A report demonstrated that the activated PI3K-Akt signaling pathway accelerates tumor cell proliferation, invasion, and metastasis, inhibiting apoptosis [46]. Furthermore, it was found that the Akt1 target was overexpressed in 15 out of 24 human hepatocellular carcinomas (63.3%) confirmed using PCR analysis through Northern blot [47]. Another research study suggested that the PI3K-Akt signaling pathway's antagonists are potential anti-cancer candidates to regulate acute and chronic inflammatory responses [48].

In the S–T–B network, Urs-12-en-24-oic acid, 3-oxo-, methyl ester had the highest degree of value and was considered the uppermost bioactive of the *C. maackii* flower against cancer. Urs-12-en-24-oic acid, 3-oxo-, methyl ester is categorized into boswellic acids used widely as anti-inflammatory agents, including as an anti-cancer treatment. Additionally, the boswellic acids have potent anti-cancer efficacy against diverse malignant cancers [49,50]. The KEGG pathway enrichment analysis of 24 targets suggested that a total of 20 signaling pathways were involved in cancer occurrence and development. The relationships of the 20 signaling pathways with cancer are concisely discussed as follows. In the Peroxisome Proliferator-Activated Receptor (PPAR) signaling pathway, the activation of the PPAR signaling pathway functions as an anti-inflammatory agent, which can overwhelm the metabolic energy balance of cancer cells by inhibiting the fatty acid synthesis and accelerating fatty acid oxidation [51,52]. In the Mitogen-Activated Protein Kinase (MAPK) signaling pathway, MAPK inhibitors are efficient blockers to reduce pro-inflammatory cytokines and enhance the anti-cancer effect, particularly on human pancreatic cancer cells [53,54]. In the Rap1 (Ras-associated protein-1) signaling pathway, Rap1 promotes cytokine production during the inflammatory condition, which leads to tumor progression in human colorectal cancer [55,56]. Regarding the calcium signaling pathway, calcium is a significant second messenger to regulate inflammation; hence, blockers of the calcium channel can induce cancer cell death [57,58]. In the Cyclic AMP (cAMP) signaling pathway, an increased cAMP level has an anti-inflammatory effect, where the increased level can regulate DNA damage, DNA repair, and apoptosis of cancer cells [59,60]. Concerning the Hypoxia-Inducible Factor-1 (HIF-1) signaling pathway, HIF-1 is a central regulator to stimulate the production of inflammation. HIF-1 overexpression is related to increased tumor growth [61,62]. In the sphingolipid signaling pathway, sphingolipid

is implicated in the inflammatory response, which has been involved in cancer cell proliferation [63,64]. In the Phospholipase D (PLD) signaling pathway, PLD inhibition can induce two functions, namely anti-inflammation and anti-cancer. Mainly, the blocking of PLD during chemotherapy can sensitize one to chemotherapeutics [65,66]. Regarding the Phosphoinositide 3-kinase-Akt (PI3K-Akt) signaling pathway, inhibition of the PI3K-Akt signaling pathway reduces the severity of inflammation in mice. This strategy is a promising mechanism for the treatment of cancers such as lung cancer, colorectal cancer, renal cancer, prostate cancer, triple-negative breast cancer, mucinous adenocarcinoma of the ovary, and skin cancer [67,68]. In the AMP-activated protein kinase (AMPK) signaling pathway, AMPK activation suppresses inflammatory responses and dampens cancer growth with cell metabolism and the cell cycle [69,70]. Regarding the Vascular Endothelial Growth Factor (VEGF) signaling pathway, VEGF is a core mediator in the formation of new blood vessels for cancer cells; thereby, cancer cells can survive, grow, and metastasize [71]. In the B cell receptor (BCR) signaling pathway, B cells are involved in the inflammatory T cell receptor, which is implicated in antibody production [72]. B cells or BCR-associated kinases may function with anti-cancer activity via B cells activation [73]. In the Fc epsilon RI signaling pathway, the expression of Fc epsilon on mast cells stimulates immunoglobulin E, leading to type 1 hypersensitivity-induced local inflammatory responses at the tumor sites [74]. In the insulin signaling pathway, insulin-resistant patients undergo excessive production of reactive oxygen species (ROS) that can harm DNA attributed to carcinogenesis [75]. In the estrogen signaling pathway, estrogen exposure to chronic inflammatory disease activity is a key risk in breast cancer progression [76]. With regards to the prolactin signaling pathway, prolactin functions as a cytokine immune system, especially in breast cancer, which has the strongest correlation with an increased expression level of prolactin and prolactin receptors [77,78]. In the thyroid signaling pathway, the optimal regulation of the cellular thyroid hormone is essential for an adequate role of immune cells during inflammation [79]. In terms of the adipocytokine signaling pathway, adipocytokine is an inflammatory mediator during immune-associated diseases, which accelerates cancer progression and metastasizes from organ to organ [80]. In the Relaxin signaling pathway, Relaxin alleviates the inflammatory severity and diminishes the amount of leucocytes and the expression level of cytokines [81]. In terms of the Advanced Glycation End-product (AGE)-Advanced Glycation End-product Receptor (RAGE) signaling pathway in diabetic complications, RAGE can stimulate inflammatory responses by binding with AGEs [82]. The inhibitor (papaverine) of RAGE is a promising target for anti-cancer activity, which blocks nuclear factor kappa B (NF- κ B) [83].

4. Materials and Methods

4.1. Plant Material Collection and Identification

The *C. maackii* flowers were collected from Mihogil of Bomunmyeon (Latitude: 36.666149, Longitude: 128.511759), Gyeongsang-bukdo, Republic of Korea, in October 2020, and the plant was identified by Dr. Dong Ha Cho, Plant biologist and Professor, Department of Bio-Health Convergence, College of Biomedical Science, Kangwon National University. A voucher number (CNB 015) has been deposited at the Kenaf Corporation in the Department of Bio-Health Convergence, and the material can only be used as research.

4.2. Plant Preparation, Extraction

The *C. maackii* flower was dried in a shady area at room temperature (20–22 °C) for 7 days, and dried leaves were powdered using an electric blender (Shinil, Cheonan, Korea). Approximately 50 g of *C. maackii* flower powder was soaked in 800 mL of 100% methanol (Daejung, Seohaean, Korea) for 5 days and repeated 3 times to collect extraction. The solvent extract was collected, filtered, and evaporated using a vacuum evaporator (RV8, IKA, Staufen, German). The evaporated sample was dried under a boiling water bath (HB10, IKA, Staufen, German) at 40 °C to obtain the extract.

4.3. GC-MS Analysis Condition

Agilent 7890A (Agilent, Santa Clara, CA, USA) was used to carry out the GC-MS analysis. GC was equipped with a DB-5 (30 m × 0.25 mm × 0.25 μm) capillary column (Agilent, Santa Clara, CA, USA). Initially, the instrument was maintained at a temperature of 100 °C for 2.1 min. The temperature rose to 300 °C at a rate of 25 °C/min and was maintained for 20 min. The injection port temperature and helium flow rate were sustained at 250 °C and 1.5 mL/min, respectively. The ionization voltage was 70 eV. The samples were injected in the split mode at 10:1. The MS scan range was set at 35–900 (*m/z*). The fragmentation patterns of mass spectra were compared with those stored in the W8N05ST Library MS database. The percentage of each compound was calculated from the relative peak area of each compound in the chromatogram. The concept of integration was used with the ChemStation integrator (Agilent, Santa Clara, CA, USA) algorithms (analyzed 19 May 2021) [84].

4.4. Bioactives Database Construction and Drug-Likeness Property

The bioactives from the *C. maackii* flower were identified by utilizing GC-MS analysis. Then, the GC-MS-detected bioactives were filtered in accordance with Lipinski's rules through SwissADME (<http://www.swissadme.ch/>) (accessed on 3 June 2021) to confirm the "Drug-likeness" physicochemical properties. PubChem (<https://pubchem.ncbi.nlm.nih.gov/>) (accessed on 3 June 2021) was utilized to select the SMILES (Simplified Molecular Input Line Entry System) bioactives.

4.5. Target Targets Related to Selected Bioactives or Cancer

Targets connected to the bioactives were selected through both the Similarity Ensemble Approach (SEA) (<http://sea.bkslab.org/>) (accessed on 7 June 2021) [85] and Swiss Target Prediction (STP) (<http://www.swisstargetprediction.ch/>) (accessed on 9 June 2021) [86] with the "Homo Sapiens" setting, both of which are based on SMILES. The cancer-related targets in humans were obtained with keywords (cancer/tumor/neoplasia/carcinoma) from TTD (<http://db.idrblab.net/ttd/>) (accessed on 12 June 2021) and OMIM (<https://www.omim.org/>) (accessed on 13 June 2021). The overlapping targets between compounds of the *C. maackii* flower and cancer targets were illustrated by VENNY 2.1 (<https://bioinfogp.cnb.csic.es/tools/venny/>) (accessed on 14 June 2021).

4.6. Construction of PPI Networks and Bubble Chart

For the final overlapping targets, STRING (<https://string-db.org/>) (accessed on 16 June 2021) [87] was utilized to analyze the PPI network. Thereby, RPackage was used to identify the degree of value. Then, signaling pathways on STRING were visualized by RPackage, a hub signaling pathway (lowest rich factor) related to a hub target (highest degree of value from PPI).

4.7. Construction of a Size Map on S-T-B Network

Both the hub target (the highest degree of value among 20 signaling pathways) and the uppermost bioactive were identified via the S–T–B network. The S–T–B networks were utilized to construct a size map, based on the degree of values. In this size map, green rectangles (nodes) represented signaling pathways, pink triangles (nodes) represented targets, and orange circles (nodes) represented bioactives. The circle size represented the degree value, the size of pink triangles represented the number of connectivity with signaling pathways, and the size of orange circles represented the number of connections with targets. The merged networks were constructed using RPackage.

4.8. Preparation for MDT of Targets

Four targets of a hub signaling pathway, i.e., Akt1 (PDB ID: 5KCV), VEGFA (PDB ID: 3V2A), PRKCA (PDB ID: 3IW4), and PHLPP1 (PDB ID: N/A), were selected on STRING via RCSB PDB (<https://www.rcsb.org/>) (accessed on 19 June 2021). Specifically, the PHLPP1

protein structure was not determined; thereby, the PDB ID was not uploaded in the .pdb format. Thus, the final three proteins selected in the .pdb format were converted into the .pdbqt format via Autodock (<http://autodock.scripps.edu/>) (accessed on 22 June 2021) [88].

4.9. Preparation for MDT of Positive Standard Ligands

A total of 13 positive control compounds on Akt1 antagonists, i.e., MK-2206 dihydrochloride (PubChem ID: 46930998), Gsk-690693 (PubChem ID: 16725726), Ipatasertib (PubChem ID: 24788740), Capiwasertib (PubChem ID: 25227436), AT7867 (PubChem ID: 11175137), A-674563 (PubChem ID: 11314340), Miransertib (PubChem ID: 53262401), BAY1125976 (PubChem ID: 70817911), Akti-1/2 (PubChem ID: 135398501), Uprosertib (PubChem ID: 51042438), Afuresertib (PubChem ID: 46843057), AT13148 (PubChem ID: 24905401), and Oridonin (PubChem ID: 5321010), were selected to verify the docking score.

4.10. Preparation for MDT of Ligand Molecules

The ligand molecules were converted from sdf in PubChem into the .pdb format using Pymol, and the ligand molecules were converted into the .pdbqt format through Autodock.

4.11. Ligand-Protein Docking

The ligand molecules were docked with targets utilizing autodock4 by setting up an energy range of 4 and exhaustiveness at 8 as the default to obtain 10 different positions of ligand molecules [89]. The center (the position of the middle coordinate point) in the target was X: −12.677, Y: 2.931, Z: −13.145 on AKT1 (PDB ID: 5KCV). The grid box size was set to 40 Å × 40 Å × 40 Å. The 2D binding interactions were used with LigPlot+ v.2.2 (<https://www.ebi.ac.uk/thornton-srv/software/LigPlus/>) (accessed on 23 June 2021) [90]. After docking, ligands of the lowest binding energy (highest affinity) were selected to visualize the ligand–protein interaction in Pymol.

4.12. Toxicological Properties Prediction by admetSAR

Toxicological properties of the key bioactive were established using the admetSAR web-service tool (<http://lmmd.ecust.edu.cn/admetSar1/predict/>) (accessed on 24 June 2021) [91] because toxicity is an essential factor in developing new drugs. Hence, Ames toxicity, carcinogenic properties, acute oral toxicity, and rat acute toxicity were predicted by admetSAR.

5. Conclusions

The bioactives and mechanisms of *C. maackii* flowers against cancer were firstly uncovered through network pharmacology. The findings suggested that 20 signaling pathways, 24 targets, and 19 bioactives are connected to cancer. Of these, the PI3K-Akt signaling pathway, Akt1, and Urs-12-en-24-oic acid, 3-oxo-, methyl ester were the hub signaling pathway, hub target, and key bioactive of *C. maackii* flowers against cancer, respectively. Furthermore, Urs-12-en-24-oic acid, 3-oxo-, methyl ester has the most potent efficacy on the Akt1 target protein than 13 other standard ligands. This study suggests that the mechanism of the *C. maackii* flower against cancer might strengthen anti-inflammatory responses by inactivating the PI3K-Akt signaling pathway, bound to Urs-12-en-24-oic acid, 3-oxo-, methyl ester on Akt1. From this viewpoint, we propose that *C. maackii* flowers can be utilized as functional or medicinal resources against cancer.

Supplementary Materials: The following are available online, Table S1: The 309, 396, and 108 targets from SEA, STP, and overlapping targets between SEA and STP, respectively. Table S2: The 4245 cancer-related targets from TTD and OMIM databases, Table S3: The final 51 targets against cancer.

Author Contributions: Conceptualization, methodology, formal analysis, investigation, visualization, data curation, writing—original draft, K.-K.O.; software, investigation, data curation, K.-K.O.

and M.A.; validation, writing—review and editing, M.A.; supervision, project administration, D.-H.C. All authors have read and agreed to the published version of the manuscript.

Funding: This research did not receive any specific grant from funding agencies in the public, commercial, or not-for-profit sectors.

Institutional Review Board Statement: Not applicable.

Informed Consent Statement: Not applicable.

Data Availability Statement: All data generated or analyzed during this study are included in this published article (and its Supplementary Information Files).

Acknowledgments: This research was acknowledged by the Department of Bio-Health Convergence, College of Biomedical Science, Kangwon National University, Chuncheon 24341, Korea.

Conflicts of Interest: There is no conflict of interest.

Sample Availability: Samples of described compounds are available from the authors.

Abbreviations

ADME	Absorption: Distribution, Metabolism, Excretion;
AGE	Advanced Glycation End-product;
AMPK	AMP-activated protein kinase;
cAMP	Cyclic AMP;
<i>C. maackii</i>	<i>Cirsium japonicum</i> var. <i>maackii</i> (Maxim.) Matsum.: <i>C. maackii</i> ;
DLCs	Drug-Like Compounds;
BCR	B cell receptor;
GC-MS	Gas Chromatography Mass Spectrum;
HIF-1	Hypoxia Inducible Factor-1;
KEGG	Kyoto Encyclopedia of Genes and Genomes;
MAPK	Mitogen Activated Protein Kinase;
MDT	Molecular Docking Test;
NF- κ B	Nuclear Factor Kappa B;
OMIM	Online Mendelian Inheritance in Man;
PI3K-Akt	Phosphoinositide 3-kinase-Akt;
PLD	Phospholipase D;
PPAR	Peroxisome Proliferator Activated Receptor;
PPI	Protein-protein interaction;
RAGE	Advanced Glycation End-product Receptor;
Rap1	Ras-associated protein-1;
ROS	Reactive Oxygen Species;
SEA	Similarity Ensemble Approach;
SMILES	Simplified Molecular Input Line Entry System;
S-T-B	Signaling pathway-Target protein-Bioactive;
STP	SwissTargetPrediction;
t-BHP	Tert-butyl hydroperoxide;
TTD	Therapeutic Target Database;
VEGF	Vascular Endothelial Growth Factor

References

1. Bertram, J.S. The molecular biology of cancer. *Mol. Asp. Med.* **2000**, *21*, 167–223. [[CrossRef](#)]
2. Nakad, R.; Schumacher, B. DNA Damage Response and Immune Defense: Links and Mechanisms. *Front. Genet.* **2016**, *7*, 147. [[CrossRef](#)]
3. Welsh, C.; Day, R.; McGurk, C.; Masters, J.R.; Wood, R.D.; Köberle, B. Reduced levels of XPA, ERCC1 and XPF DNA repair proteins in testis tumor cell lines. *Int. J. Cancer* **2004**, *110*, 352–361. [[CrossRef](#)] [[PubMed](#)]
4. Munn, L.L. Cancer and inflammation. *Wiley Interdiscip. Rev. Syst. Biol. Med.* **2017**, *9*, e1370. [[CrossRef](#)] [[PubMed](#)]
5. Lacourt, T.E.; Vichaya, E.G.; Chiu, G.S.; Dantzer, R.; Heijnen, C.J. The high costs of low-grade inflammation: Persistent fatigue as a consequence of reduced cellular-energy availability and non-adaptive energy expenditure. *Front. Behav. Neurosci.* **2018**, *12*, 78. [[CrossRef](#)]

6. Coussens, L.M.; Werb, Z. Inflammation and cancer. *Nature* **2002**, *420*, 860–867. [[CrossRef](#)]
7. Rayburn, E.R.; Ezell, S.J.; Zhang, R. Anti-inflammatory agents for cancer therapy. *Mol. Cell. Pharmacol.* **2009**, *1*, 29–43. [[CrossRef](#)]
8. Subramaniam, M.; Liew, S.K.; In, L.L.; Awang, K.; Ahmed, N.; Nagoor, N.H. Inactivation of nuclear factor κ B by MIP-based drug combinations augments cell death of breast cancer cells. *Drug Des. Dev. Ther.* **2018**, *12*, 1053–1063. [[CrossRef](#)]
9. Shewach, D.S.; Kuchta, R.D. Introduction to Cancer Chemotherapeutics. *Chem. Rev.* **2009**, *109*, 2859–2861. [[CrossRef](#)]
10. Kayl, A.E.; Meyers, C.A. Side-effects of chemotherapy and quality of life in ovarian and breast cancer patients. *Curr. Opin. Obstet. Gynecol.* **2006**, *18*, 24–28. [[CrossRef](#)]
11. Aravindaram, K.; Yang, N.-S. Anti-Inflammatory Plant Natural Products for Cancer Therapy. *Planta Medica* **2010**, *76*, 1103–1117. [[CrossRef](#)] [[PubMed](#)]
12. Greenwell, M.; Rahman, P. Medicinal Plants: Their Use in Anticancer Treatment. *Int. J. Pharm. Sci. Res.* **2015**, *6*, 4103–4112. [[CrossRef](#)] [[PubMed](#)]
13. Desai, A.G.; Qazi, G.N.; Ganju, R.K.; El-Tamer, M.; Singh, J.; Saxena, A.K.; Bedi, Y.S.; Taneja, S.C.; Bhat, H.K. Medicinal Plants and Cancer Chemoprevention. *Curr. Drug Metab.* **2008**, *9*, 581–591. [[CrossRef](#)] [[PubMed](#)]
14. Wagle, A.; Seong, S.H.; Shrestha, S.; Jung, H.A.; Choi, J.S. Korean Thistle (*Cirsium japonicum* var. *maackii* (Maxim.) Matsum.): A Potential Dietary Supplement against Diabetes and Alzheimer’s Disease. *Molecules* **2019**, *24*, 649. [[CrossRef](#)]
15. Nazaruk, J.; Wajs-Bonikowska, A.; Bonikowski, R. Components and antioxidant activity of fruits of *Cirsium palustre* and *C. rivulare*. *Chem. Nat. Compd.* **2012**, *48*, 8–10. [[CrossRef](#)]
16. Kim, E.-Y.; Jho, H.-K.; Kim, N.-I.; Rhyu, M.R. *Cirsium japonicum* elicits endothelium-dependent relaxation via histamine H1-receptor in rat thoracic aorta. *J. Ethnopharmacol.* **2008**, *116*, 223–227. [[CrossRef](#)]
17. Liu, S.; Zhang, J.; Li, D.; Liu, W.; Luo, X.; Zhang, R.; Li, L.; Zhao, J. Anticancer activity and quantitative analysis of flavone of *Cirsium japonicum* DC. *Nat. Prod. Res.* **2007**, *21*, 915–922. [[CrossRef](#)]
18. Ma, Q.; Guo, Y.; Luo, B.; Liu, W.; Wei, R.; Yang, C.; Ding, C.; Xu, X.; He, M. Hepatoprotective phenylethanoid glycosides from *Cirsium setosum*. *Nat. Prod. Res.* **2015**, *30*, 1824–1829. [[CrossRef](#)]
19. Park, J.Y.; Kim, H.Y.; Shibamoto, T.; Jang, T.S.; Lee, S.C.; Shim, J.S.; Hahm, D.-H.; Lee, H.-J.; Lee, S.; Kang, K.S. Beneficial effects of a medicinal herb, *Cirsium japonicum* var. *maackii*, extract and its major component, cirsimaritin on breast cancer metastasis in MDA-MB-231 breast cancer cells. *Bioorg. Med. Chem. Lett.* **2017**, *27*, 3968–3973. [[CrossRef](#)] [[PubMed](#)]
20. Jung, H.A.; Abdul, Q.A.; Byun, J.S.; Joung, E.-J.; Gwon, W.-G.; Lee, M.-S.; Kim, H.-R.; Choi, J.S. Protective effects of flavonoids isolated from Korean milk thistle *Cirsium japonicum* var. *maackii* (Maxim.) Matsum on *tert*-butyl hydroperoxide-induced hepatotoxicity in HepG2 cells. *J. Ethnopharmacol.* **2017**, *209*, 62–72. [[CrossRef](#)]
21. Gartung, A.; Yang, J.; Sukhatme, V.P.; Bielenberg, D.R.; Fernandes, D.; Chang, J.; Schmidt, B.A.; Hwang, S.H.; Zurakowski, D.; Huang, S.; et al. Suppression of chemotherapy-induced cytokine/lipid mediator surge and ovarian cancer by a dual COX-2/sEH inhibitor. *Proc. Natl. Acad. Sci. USA* **2019**, *116*, 1698–1703. [[CrossRef](#)] [[PubMed](#)]
22. Bhatarrai, G.; Seong, S.H.; Jung, H.A.; Choi, J.S. Isolation and Quantitative Analysis of BACE1 Inhibitory Compounds from *Cirsium maackii* Flower. *Nat. Prod. Sci.* **2019**, *25*, 326–333. [[CrossRef](#)]
23. Aral, H.; Aral, T.; Çelik, K.S.; Ziyadanoğulları, B.; Ziyadanoğulları, R. HPLC Separation of Different Groups of Small Polar Compounds on a Novel Amide-Embedded Stationary Phase. *Chromatographia* **2014**, *77*, 771–781. [[CrossRef](#)]
24. De La Torre, M.P.D.; Priego-Capote, F.; De Castro, M.D.L. Tentative identification of polar and mid-polar compounds in extracts from wine lees by liquid chromatography-tandem mass spectrometry in high-resolution mode. *J. Mass Spectrom.* **2015**, *50*, 826–837. [[CrossRef](#)] [[PubMed](#)]
25. Constantinescu, T.; Lungu, C.N.; Lung, I. Lipophilicity as a Central Component of Drug-Like Properties of Chalcones and Flavonoid Derivatives. *Molecules* **2019**, *24*, 1505. [[CrossRef](#)] [[PubMed](#)]
26. Sympli, H.D. Estimation of drug-likeness properties of GC–MS separated bioactive compounds in rare medicinal *Pleione maculata* using molecular docking technique and SwissADME in silico tools. *Netw. Model. Anal. Heal. Informatics Bioinform.* **2021**, *10*, 1–36. [[CrossRef](#)]
27. Oh, K.K.; Adnan, M.; Cho, D.H. Network pharmacology of bioactives from *Sorghum bicolor* with targets related to diabetes mellitus. *PLoS ONE* **2020**, *15*, e0240873. [[CrossRef](#)]
28. Hopkins, A.L. Network pharmacology: The next paradigm in drug discovery. *Nat. Chem. Biol.* **2008**, *4*, 682–690. [[CrossRef](#)]
29. Wang, Y.; Hu, B.; Feng, S.; Wang, J.; Zhang, F. Target recognition and network pharmacology for revealing anti-diabetes mechanisms of natural product. *J. Comput. Sci.* **2020**, *45*, 101186. [[CrossRef](#)]
30. Ye, H.; Wei, J.; Tang, K.; Feuers, R.; Hong, H. Drug Repositioning Through Network Pharmacology. *Curr. Top. Med. Chem.* **2016**, *16*, 3646–3656. [[CrossRef](#)]
31. Kibble, M.; Saarinen, N.; Tang, J.; Wennerberg, K.; Mäkelä, S.; Aittokallio, T. Network pharmacology applications to map the unexplored target space and therapeutic potential of natural products. *Nat. Prod. Rep.* **2015**, *32*, 1249–1266. [[CrossRef](#)]
32. Nisa, S.; Khan, N.; Shah, W.; Sabir, M.; Khan, W.; Bibi, Y.; Jahangir, M.; Haq, I.U.; Alam, S.; Qayyum, A. Identification and Bioactivities of Two Endophytic Fungi *Fusarium fujikuroi* and *Aspergillus tubingensis* from Foliar Parts of *Debregeasia salicifolia*. *Arab. J. Sci. Eng.* **2020**, *45*, 4477–4487. [[CrossRef](#)]
33. Bassole, I.H.N.; Nebie, R.; Savadogo, A.; Ouattara, C.T.; Barro, N.; Traore, S.A. Composition and antimicrobial activities of the leaf and flower essential oils of *Lippia chevalieri* and *Ocimum canum* from Burkina Faso. *Afr. J. Biotechnol.* **2005**, *4*, 1156–1160. [[CrossRef](#)]

34. Lee, J.-Y.; Lee, H.-J.; Jeong, J.-A.; Jung, J.-W. Palmitic acid inhibits inflammatory responses in lipopolysaccharide-stimulated mouse peritoneal macrophages. *Orient. Pharm. Exp. Med.* **2010**, *10*, 37–43. [CrossRef]
35. Sebastianes, F.L.S.; Cabedo, N.; El Aouad, N.; Valente, A.M.M.P.; Lacava, P.T.; Azevedo, J.L.; Pizzirani-Kleiner, A.A.; Cortes, D. 3-Hydroxypropionic Acid as an Antibacterial Agent from Endophytic Fungi *Diaporthe phaseolorum*. *Curr. Microbiol.* **2012**, *65*, 622–632. [CrossRef] [PubMed]
36. Cardoso, V.M.; Solano, A.G.R.; Prado, M.A.F.; Nunan, E.D.A. Investigation of fatty acid esters to replace isopropyl myristate in the sterility test for ophthalmic ointments. *J. Pharm. Biomed. Anal.* **2006**, *42*, 630–634. [CrossRef]
37. Ivanova, E.P.; Nguyen, S.H.; Guo, Y.; Baulin, V.; Webb, H.; Truong, V.K.; Wandiyanto, J.V.; Garvey, C.J.; Mahon, P.; Mainwaring, D.E.; et al. Bactericidal activity of self-assembled palmitic and stearic fatty acid crystals on highly ordered pyrolytic graphite. *Acta Biomater.* **2017**, *59*, 148–157. [CrossRef]
38. Maruthi, R.; Chandan, R.; Barath, M.; Datta, G.N.; D’Silva, M.; Kumari, M.K.; Ahmad, F.; Geetha, R. Analytical method development and validation of teneligliptin by rp-uflc. *Res. J. Pharm. Technol.* **2020**, *13*, 4035. [CrossRef]
39. PCIDB. Available online: <https://www.genome.jp/db/pcidb> (accessed on 19 March 2021).
40. Pédebooscq, S.; Rey, C.; Petit, M.; Harpey, C.; De Giorgi, F.; Ichas, F.; Lartigue, L. Non-Antioxidant Properties of α -Tocopherol Reduce the Anticancer Activity of Several Protein Kinase Inhibitors In Vitro. *PLoS ONE* **2012**, *7*, e36811. [CrossRef] [PubMed]
41. Oh, K.K.; Adnan, M.; Ju, I.; Cho, D.H. A network pharmacology study on main chemical compounds from *Hibiscus cannabinus* L. leaves. *RSC Adv.* **2021**, *11*, 11062–11082. [CrossRef]
42. Zhong, R.-F.; Xu, G.-B.; Wang, Z.; Wang, A.-M.; Guan, H.-Y.; Li, J.; He, X.; Liu, J.-H.; Zhou, M.; Li, Y.-J.; et al. Identification of anti-inflammatory constituents from *Kalimeris indica* with UHPLC-ESI-Q-TOF-MS/MS and GC-MS. *J. Ethnopharmacol.* **2015**, *165*, 39–45. [CrossRef]
43. Wonkam, A.K.N.; Ngansop, C.A.N.; Wouamba, S.C.N.; Jouda, J.B.; Happi, G.M.; Boyom, F.F.; Sewald, N.; Lenta, B.N. Rothmannamide and other constituents from the leaves of *Rothmannia hispida* (K.Schum.) fagerl. (Rubiaceae) and their chemophenetic significance. *Biochem. Syst. Ecol.* **2020**, *93*, 104137. [CrossRef]
44. Kühnl, A.; Musiol, A.; Heitzig, N.; Johnson, D.E.; Ehrhardt, C.; Grewal, T.; Gerke, V.; Ludwig, S.; Rescher, U. Late Endosomal/Lysosomal Cholesterol Accumulation Is a Host Cell-Protective Mechanism Inhibiting Endosomal Escape of Influenza A Virus. *mBio* **2018**, *9*. [CrossRef] [PubMed]
45. Mohan, R.; Wilson, M.; Gorham, R.; Harrison, R.E.S.; Morikis, V.A.; Kieslich, C.; Orr, A.A.; Coley, A.V.; Tamamis, P.; Morikis, D. Virtual Screening of Chemical Compounds for Discovery of Complement C3 Ligands. *ACS Omega* **2018**, *3*, 6427–6438. [CrossRef]
46. Liu, R.; Chen, Y.; Liu, G.; Li, C.; Song, Y.; Cao, Z.; Li, W.; Hu, J.; Lu, C.; Liu, Y. PI3K/AKT pathway as a key link modulates the multidrug resistance of cancers. *Cell Death Dis.* **2020**, *11*, 1–12. [CrossRef] [PubMed]
47. Liu, L.-X.; Liu, Z.-H.; Jiang, H.-C.; Qi, S.-Y.; Zhang, W.-H.; Zhu, A.-L.; Wang, X.-Q.; Wu, M. Overexpression of Akt-1 gene in human hepatocellular carcinoma. *Chin. J. Cancer Res.* **2002**, *14*, 161–164. [CrossRef]
48. Di Lorenzo, A.; Fernandez-Hernando, C.; Cirino, G.; Sessa, W.C. Akt1 is critical for acute inflammation and histamine-mediated vascular leakage. *Proc. Natl. Acad. Sci. USA* **2009**, *106*, 14552–14557. [CrossRef]
49. Chenniappan, J.; Sankaranarayanan, A.; Arjunan, S. Evaluation of Antimicrobial Activity of *Cissus quadrangularis* L. stem extracts against Avian Pathogens and Determination of its Bioactive Constituents using GC-MS. *J. Sci. Res.* **2020**, *64*, 90–96. [CrossRef]
50. Sharma, T.; Jana, S. Boswellic acids as natural anticancer medicine: Precious gift to humankind. *J. Herb. Med.* **2020**, *20*, 100313. [CrossRef]
51. Fuentes, E.; Guzmán-Jofre, L.; Moore-Carrasco, R.; Palomo, I. Role of PPARs in inflammatory processes associated with metabolic syndrome (Review). *Mol. Med. Rep.* **2013**, *8*, 1611–1616. [CrossRef]
52. Grabacka, M.; Reiss, K. Anticancer Properties of PPAR α -Effects on Cellular Metabolism and Inflammation. *PPAR Res.* **2008**, *2008*, 930705. [CrossRef]
53. Kaminska, B. MAPK signalling pathways as molecular targets for anti-inflammatory therapy—From molecular mechanisms to therapeutic benefits. In Proceedings of the Biochimica et Biophysica Acta—Proteins and Proteomics, Warsaw, Poland, 25–29 June 2005; pp. 253–262.
54. Qian, C.; Qi, Y.; Zhong, S.; Zeng, J.; Chen, X.; Yao, J. Mitogen-activated protein kinase inhibition enhances the antitumor effects of sporamin in human pancreatic cancer cells. *Oncol. Lett.* **2018**, *16*, 1237–1242. [CrossRef]
55. Cai, Y.; Sukhova, G.K.; Wong, H.K.; Xu, A.; Tergaonkar, V.; Vanhoutte, P.M.; Tang, E.H.C. Rap1 induces cytokine production in pro-inflammatory macrophages through NF κ B signaling and is highly expressed in human atherosclerotic lesions. *Cell Cycle* **2015**, *14*, 3580–3592. [CrossRef]
56. Gao, W.; Ye, G.; Liu, L.; Wei, L. The downregulation of Rap1 GTPase-activating protein is associated with a poor prognosis in colorectal cancer and may impact on tumor progression. *Oncol. Lett.* **2018**, *15*, 7661–7668. [CrossRef]
57. Dalal, P.J.; Muller, W.A.; Sullivan, D.P. Endothelial Cell Calcium Signaling during Barrier Function and Inflammation. *Am. J. Pathol.* **2020**, *190*, 535–542. [CrossRef]
58. Bong, A.H.; Monteith, G.R. Calcium signaling and the therapeutic targeting of cancer cells. *Biochim. Biophys. Acta (BBA)—Mol. Cell Res.* **2018**, *1865*, 1786–1794. [CrossRef]
59. Erdogan, S.; Aslantas, O.; Celik, S.; Atik, E. The effects of increased cAMP content on inflammation, oxidative stress and PDE4 transcripts during *Brucella melitensis* infection. *Res. Vet. Sci.* **2008**, *84*, 18–25. [CrossRef]

60. Zou, T.; Liu, J.; She, L.; Chen, J.; Zhu, T.; Yin, J.; Li, X.; Li, X.; Zhou, H.; Liu, Z. A perspective profile of ADCY1 in cAMP signaling with drug-resistance in lung cancer. *J. Cancer* **2019**, *10*, 6848–6857. [[CrossRef](#)] [[PubMed](#)]
61. Gaspar, J.M.; Velloso, L.A. Hypoxia inducible factor as a central regulator of metabolism—Implications for the development of obesity. *Front. Neurosci.* **2018**, *12*, 813. [[CrossRef](#)] [[PubMed](#)]
62. Semenza, G.L. Evaluation of HIF-1 inhibitors as anticancer agents. *Drug Discov. Today* **2007**, *12*, 853–859. [[CrossRef](#)] [[PubMed](#)]
63. Nixon, G.F. Sphingolipids in inflammation: Pathological implications and potential therapeutic targets. *Br. J. Pharmacol.* **2009**, *158*, 982–993. [[CrossRef](#)] [[PubMed](#)]
64. Ponnusamy, S.; Meyers-Needham, M.; Senkal, C.E.; Saddoughi, S.A.; Sentelle, D.; Selvam, S.P.; Salas, A.; Ogretmen, B. Sphingolipids and cancer: Ceramide and sphingosine-1-phosphate in the regulation of cell death and drug resistance. *Futur. Oncol.* **2010**, *6*, 1603–1624. [[CrossRef](#)]
65. Kang, D.W.; Choi, K.-Y.; Min, D.S. Functional Regulation of Phospholipase D Expression in Cancer and Inflammation. *J. Biol. Chem.* **2014**, *289*, 22575–22582. [[CrossRef](#)]
66. Cho, J.H.; Han, J.-S. Phospholipase D and Its Essential Role in Cancer. *Mol. Cells* **2017**, *40*, 805–813. [[CrossRef](#)]
67. Hawkins, P.; Stephens, L. PI3K signalling in inflammation. *Biochim. Biophys. Acta (BBA)—Mol. Cell Biol. Lipids* **2015**, *1851*, 882–897. [[CrossRef](#)]
68. Yang, J.; Nie, J.; Ma, X.; Wei, Y.; Peng, Y.; Wei, X. Targeting PI3K in cancer: Mechanisms and advances in clinical trials. *Mol. Cancer* **2019**, *18*, 1–28. [[CrossRef](#)]
69. Chen, X.; Li, X.; Zhang, W.; He, J.; Xu, B.; Lei, B.; Wang, Z.; Cates, C.; Rousselle, T.; Li, J. Activation of AMPK inhibits inflammatory response during hypoxia and reoxygenation through modulating JNK-mediated NF- κ B pathway. *Metabolism* **2018**, *83*, 256–270. [[CrossRef](#)] [[PubMed](#)]
70. Chuang, H.-C.; Chou, C.-C.; Kulp, S.; Chen, C.-S. AMPK as a Potential Anticancer Target—Friend or Foe? *Curr. Pharm. Des.* **2014**, *20*, 2607–2618. [[CrossRef](#)] [[PubMed](#)]
71. Carmeliet, P. VEGF as a Key Mediator of Angiogenesis in Cancer. *Oncology* **2005**, *69*, 4–10. [[CrossRef](#)] [[PubMed](#)]
72. Zeng, Q.-H.; Wei, Y.; Lao, X.-M.; Chen, D.-P.; Huang, C.-X.; Lin, Q.-Y.; He, M.; Liao, Y.; Zheng, L.; Li, B.; et al. B cells polarize pathogenic inflammatory T helper subsets through ICOSL-dependent glycolysis. *Sci. Adv.* **2020**, *6*, eabb6296. [[CrossRef](#)] [[PubMed](#)]
73. Burger, J.A.; Wiestner, A. Targeting B cell receptor signalling in cancer: Preclinical and clinical advances. *Nat. Rev. Cancer* **2018**, *18*, 148–167. [[CrossRef](#)]
74. Luiten, R.M.; Warnaar, S.O.; Schuurman, J.; Pasmans, S.G.; Latour, S.; Daëron, M.; Fleuren, G.J.; Litvinov, S.V. Chimeric immunoglobulin E reactive with tumor-associated antigen activates human Fc ϵ RI bearing cells. *Hum. Antibodies* **1997**, *8*, 169–180. [[CrossRef](#)]
75. Arcidiacono, B.; Iiritano, S.; Nocera, A.; Possidente, K.; Nevolo, M.T.; Ventura, V.; Foti, D.; Chiefari, E.; Brunetti, A. Insulin Resistance and Cancer Risk: An Overview of the Pathogenetic Mechanisms. *Exp. Diabetes Res.* **2012**, *2012*, 1–12. [[CrossRef](#)]
76. Monteiro, R.; Teixeira, D.; Calhau, C. Estrogen Signaling in Metabolic Inflammation. *Mediat. Inflamm.* **2014**, *2014*, 615917. [[CrossRef](#)]
77. Orbach, H.; Shoenfeld, Y. Hyperprolactinemia and autoimmune diseases. *Autoimmun. Rev.* **2007**, *6*, 537–542. [[CrossRef](#)] [[PubMed](#)]
78. Sethi, B.K.; Chanukya, G.; Nagesh, V.S. Prolactin and cancer: Has the orphan finally found a home? *Indian J. Endocrinol. Metab.* **2012**, *16*, S195–S198. [[CrossRef](#)] [[PubMed](#)]
79. van der Spek, A.H.; Fliers, E.; Boelen, A. Thyroid hormone in inflammation. *Endocr. Abstr.* **2019**, *65*. [[CrossRef](#)]
80. Liu, C.; Zhao, Q.; Yu, X. Bone Marrow Adipocytes, Adipocytokines, and Breast Cancer Cells: Novel Implications in Bone Metastasis of Breast Cancer. *Front. Oncol.* **2020**, *10*, 561595. [[CrossRef](#)] [[PubMed](#)]
81. Thanasupawat, T.; Glogowska, A.; Nivedita-Krishnan, S.; Wilson, B.; Klonisch, T.; Hombach-Klonisch, S. Emerging roles for the relaxin/RXFP1 system in cancer therapy. *Mol. Cell. Endocrinol.* **2019**, *487*, 85–93. [[CrossRef](#)] [[PubMed](#)]
82. Logan, S.M.; Storey, K.B. Pro-inflammatory AGE-RAGE signaling is activated during arousal from hibernation in ground squirrel adipose. *PeerJ* **2018**, *6*, e4911. [[CrossRef](#)] [[PubMed](#)]
83. El-Far, A.; Munesue, S.; Harashima, A.; Sato, A.; Shindo, M.; Nakajima, S.; Inada, M.; Tanaka, M.; Takeuchi, A.; Tsuchiya, H.; et al. In vitro anticancer effects of a RAGE inhibitor discovered using a structure-based drug design system. *Oncol. Lett.* **2018**, *15*, 4627–4634. [[CrossRef](#)]
84. Oh, K.K.; Adnan, M.; Cho, D.H. Active ingredients and mechanisms of *Phellinus linteus* (grown on *Rosa multiflora*) for alleviation of Type 2 diabetes mellitus through network pharmacology. *Gene* **2021**, *768*, 145320. [[CrossRef](#)]
85. Keiser, M.; Roth, B.L.; Armbruster, B.N.; Ernsberger, P.; Irwin, J.; Shoichet, B.K. Relating protein pharmacology by ligand chemistry. *Nat. Biotechnol.* **2007**, *25*, 197–206. [[CrossRef](#)] [[PubMed](#)]
86. Daina, A.; Michielin, O.; Zoete, V. SwissTargetPrediction: Updated data and new features for efficient prediction of protein targets of small molecules. *Nucleic Acids Res.* **2019**, *47*, W357–W364. [[CrossRef](#)]
87. Szklarczyk, D.; Gable, A.L.; Lyon, D.; Jung, A.; Wyder, S.; Huerta-Cepas, J.; Simonovic, M.; Doncheva, N.T.; Morris, J.H.; Bork, P.; et al. STRING v11: Protein–protein association networks with increased coverage, supporting functional discovery in genome-wide experimental datasets. *Nucleic Acids Res.* **2019**, *47*, D607–D613. [[CrossRef](#)] [[PubMed](#)]
88. Morris, G.M.; Huey, R.; Lindstrom, W.; Sanner, M.F.; Belew, R.K.; Goodsell, D.S.; Olson, A.J. AutoDock4 and AutoDockTools4: Automated docking with selective receptor flexibility. *J. Comput. Chem.* **2009**, *30*, 2785–2791. [[CrossRef](#)]

-
89. Khanal, P.; Patil, B.M.; Chand, J.; Naaz, Y. Anthraquinone Derivatives as an Immune Booster and their Therapeutic Option Against COVID-19. *Nat. Prod. Bioprospect.* **2020**, *10*, 325–335. [[CrossRef](#)]
 90. Laskowski, R.A.; Swindells, M.B. LigPlot+: Multiple ligand-protein interaction diagrams for drug discovery. *ACS Pub.* **2011**, *51*, 2778–2786. [[CrossRef](#)]
 91. Yang, H.; Lou, C.; Sun, L.; Li, J.; Cai, Y.; Wang, Z.; Li, W.; Liu, G.; Tang, Y. admetSAR 2.0: Web-service for prediction and optimization of chemical ADMET properties. *Bioinformatics* **2018**, *35*, 1067–1069. [[CrossRef](#)]